The Effect of Formation Redshifts on the Cluster Mass–Temperature Relation

Benjamin F. Mathiesen

Department of Physics, Stanford University, Stanford, CA 94305-4060 USA

27 October 2018

ABSTRACT

I employ an ensemble of hydrodynamical simulations and the XSPEC MEKAL emission model to reproduce observable spectral and flux-weighted temperatures for 24 clusters. Each cluster is imaged at 16 points in its history, which allows the investigation of evolutionary effects on the mass-temperature relation. In the zero redshift scaling relations, I find no evidence for a relationship between cluster temperature and formation epoch for those clusters which acquired 75% of their final mass since a redshift of 0.6. This result holds for both observable and intrinsic intracluster medium temperatures, and implies that halo formation epochs are not an important variable in analysis of observable cluster temperature functions.

Key words: galaxies: clusters: general – large-scale structure of Universe

1 INTRODUCTION

Galaxy clusters are the youngest and largest organized structures known to exist, and their ensemble properties can shed light on many cosmological problems. They arise from significantly overdense regions on cosmological scales, which are exponentially rare events in a Gaussian initial perturbation spectrum. The shape and normalisation of the cluster mass function are therefore extremely sensitive to the statistical properties of the primordial density field. The evolution of cluster number densities is also tightly coupled to the cosmic expansion rate, and can precisely constrain Ω_m. Much effort has been expended towards a measurement of the cluster mass function and its evolution (see Henry 2000 for a summary of recent work in this area), but much remains to be understood about the clusters themselves before we can be confident of such results.

The properties of the local mass function can be constrained by using either standard Press-Schecter (1974) (also Bond et al. 1991, Lacey & Cole 1993) theory, a more sophisticated analytical model of the cosmic mass function (e.g. Sheth, Mo, & Tormen 1999), or fitting formula based on large-scale structure simulations (Jenkins et al. 2000). These methods predict the number density of dark matter haloes as a function of mass and redshift. Some relationship between model variables (i.e., the total mass within some density threshold) and a more easily observed quantity (e.g. X–ray temperature, X–ray luminosity, or weak lensing mass) must therefore be assumed to match cosmological predic-

tions to the results of cluster surveys. Intracluster medium (ICM) X–ray temperatures show particular promise in this regard, since they demonstrate a tight ($\lesssim 20\%$ scatter) correlation with cluster mass components in both simulations (Mathiesen & Evrard 2001, total mass) and observations (Mohr, Mathiesen, & Evrard 1999, ICM mass), and the cluster X–ray temperature function (XTF) currently provides the tightest constraints on the cluster mass function. It therefore seems likely that our best structure formation measurements of Ω_m will rely on medium-redshift measurements of the XTF, and it is essential to make sure that our interpretation of cluster temperature functions is correct.

A modified form of the mass function allowing for differences between a cluster's formation redshift and observed redshift was first proposed by Kitayama & Suto (1996), and has begun to be commonly implemented in deriving constraints on the power spectrum normalization σ_8 at low redshifts (Kitayama & Suto 1997, Kay & Bower 1999, Viana & Liddle 1999). This extension to the theory produces little change in the shape of the predicted mass function, but can have an appreciable effect on the predicted temperature function if one assumes that clusters scatter around a mass-temperature scaling relation appropriate to their formation redshift. This implies that clusters have objectively identifiable formation events, during which the majority of a cluster's mass coalesces for the first time and the ICM virialises at a temperature appropriate to the halo mass and formation epoch. These assumptions are reasonable in the framework of standard Press-Schechter theory, but perhaps

pay too little heed to the more complicated, hydrodynamical evolution of the ICM.

The goal of this paper is to investigate the evolution of intrinsic and observable cluster temperatures using an ensemble of 24 hydrodynamic cluster simulations, and test the appropriateness of this extension to the interpretation of cluster temperature functions. In the following section I describe the ensemble of simulated clusters and our model for the ICM X–ray emission. In section 3, I look for evidence of temperature evolution in our ensemble. Section 4 summarizes the results of this letter. The Hubble constant is parameterized as $H_0 = 100h$ km s^{-1} Mpc^{-1}.

2 SIMULATED AND OBSERVABLE TEMPERATURES

We use an ensemble of 24 hydrodynamical cluster simulations, divided evenly between two reasonable cold dark matter (CDM) cosmological models. These models are OCDM ($\Omega_0 = 0.3$, $\sigma_8 = 1.0$, $h = 0.8$, $\Gamma = 0.24$) and ΛCDM ($\Omega_0 = 0.3$, $\lambda_0 = 0.7$, $\sigma_8 = 1.0$, $h = 0.8$, $\Gamma = 0.24$). Here σ_8 is the linearly evolved, present day power spectrum normalization on $8h^{-1}$ Mpc scales. The initial conditions are Gaussian random fields consistent with a CDM transfer function with the specified Γ (e.g. Bond & Efstathiou 1984). The baryon density is set in each case to 20% of the total mass density ($\Omega_b = 0.2\Omega_0$). The simulation scheme is P3MSPH: the first stage is a P^{3}M (dark matter only) simulation to find cluster formation sites in a large volume, and the second stage resimulates the formation of individual clusters with higher resolution. Smoothed particle hydrodynamics (SPH) is included in the individual cluster simulations to resolve the ICM structure in detail. The baryonic component is modeled with 32^3 particles, providing a typical mass resolution of 0.01% within the virial radius. The resulting sample covers a little more than a decade in mass, ranging from about 10^{14} to $3 \times 10^{15} M_\odot$. These simulations were first presented a paper describing the cluster size-temperature relation (Mohr & Evrard 1997).

The simulations model the dynamical and thermodynamical effects of gravitation, shock heating and adiabatic work on the ICM. Several potentially important pieces of physics are neglected. Radiative cooling is perhaps the most significant; our clusters cannot produce cooling flows in their cores. Cooling flows have the potential to greatly influence ICM luminosity and temperature measurements, but the energy lost due to radiation is small compared to that released in the process of gravitational collapse. We therefore expect that the results of these simulations are comparable to observational results which attempt to empirically account for the presence of cooling flows, either through excision or explicit modeling of excess core emission. Other neglected processes include galaxy feedback (Metzler & Evrard 1994) which can produce abundance gradients and shallower gas profiles; preheating of the ICM (Cavaliere, Menci, & Tozzi 1998; Lloyd-Davies, Ponman, & Cannon 2000), which can raise the ICM entropy and limit the density of baryonic cores; and electron temperature lag, which slightly cools X–ray spectra in

rich clusters (Chièze, Alimi & Teyssier 1998; Takizawa 1999) relative to the ion temperature. Further discussion of these issues in terms of their relevance to cluster simulations can be found in Mathiesen & Evrard (2001, hereafter ME01) and Bialek, Evrard, & Mohr (2001).

In ME01 we introduced an ensemble of spectrally and spatially resolved X–ray surface brightness images derived from these simulations. We used the MEKAL (Mewe, Lemen, & van den Oord 1986) program from the XSPEC utility, since this is the emission model most commonly used to interpret observed ICM spectra. Each SPH particle was assigned a 0.3 solar metallicity spectrum scaled to its density and thermodynamic temperature and binned in 50 eV intervals over the [0.1,20] keV bandpass. The clusters were then "observed" by collecting photons in a circular window centered on the minimum potential of the cluster, producing a combined spectrum which incorporates emission from gas with a broad distribution of phases. We produced *Chandra*-like combined spectra and spectral images by adopting 150 eV bins, a 0.5-9.5 keV bandpass, and finally convolving the photon distribution with *Chandra's* effective area function and a moderate (3.4×10^{20} cm^{-2}) absorbing column density. The physical scale of the observation windows used in this paper varies from cluster to cluster, but usually corresponds to a fixed mean interior overdensity of 500 times the critical density appropriate to the redshift and cosmological model. This radius is labelled r_{500}, and is a fixed fraction of the virial radius in any cosmology. The radius r_{200} is also used in this work, but corresponds less closely to observable regions of the ICM.

The resulting spectra are surprisingly similar in character to isothermal spectra with a temperature typically 10-20% lower than the mass-weighted mean thermodynamic ICM temperature. A semantic separation of the two concepts appears to be necessary, so hereafter we refer to the *Chandra*-like temperature just described as a *spectral* temperature, T_s. The mass-weighted mean thermodynamic temperature will be referred to as the *virial* temperature T_v, because this measure is found to precisely follow the virial relation $M_{\rm tot} \propto T^{1.5}$ in these and other simulations. T_v is identical to the mass-weighted temperature T_m defined in ME01. When spectral fitting is limited to the 2.0-9.5 keV band (similar to most published temperature determinations) the deviation δT_s between spectral and virial temperatures follows the relation

$$\delta T_s \equiv \frac{T_v - T_s}{T_s} = (0.19 \pm 0.06) \log_{10} T_s[\text{keV}] - (0.02 \pm 0.04). \quad (1)$$

This deviation steepens the observable mass-temperature relation to $M_{\rm tot} \propto T_s^{1.62}$, and implies that rich clusters are more massive than their spectral temperatures would lead us to believe. The difference between spectral and virial temperatures arises partly from the presence of recent minor mergers in the gas column, and partly from global ICM temperature profiles. Both effects contribute cooler gas to the observation window and an overabundance of soft, line-emission photons to the spectrum. I refer the reader to ME01 for further details on this work.

The temperature bias described in Equation 1 has a

potentially important effect on any interpretation of the cluster temperature function and its evolution. As has already been stated, these simulations do not include radiative cooling and are therefore directly comparable only to X–ray data which has accounted for the presence of cooling flows through excision or explicit modeling of the excess emission. Since it has not been possible until very recently to measure the spatial extent of cooling flows in high-redshift clusters, most studies of cluster evolution have evaluated the temperature and luminosity functions at low redshifts without attempting such corrections. In such works, the additional scatter introduced into cluster scaling relations by cooling flows has been accepted as a source of uncertainty in the cosmological constraints.

With the advent of *Chandra* and *XMM*, however, we can do better. Markevitch (1998) has shown that by excising the central $50h^{-1}$ Mpc of nearby clusters and including a cooling flow component in the core spectrum, the scatter in the luminosity-temperature relation can be reduced by a factor of two. This allows for a more robust calculation of the maximum observable volume for each cluster as a function of temperature, as well as providing a cleaner estimate of the ICM temperature in cooling flow clusters. The new telescopes should allow similar corrections to be made in high-redshift clusters. In order to achieve precise cosmological constraints from a measurement of evolution in the XTF, it is therefore desirable to model such cooling flow-corrected temperatures.

Temperatures derived from high-quality *ASCA* data (Markevitch et al. 1998) are commonly used in constructing the local XTF or measuring the slope of cluster scaling relations. These are flux-weighted mean spectral temperatures, which are biased towards regions containing dense and/or cool gas. This measure was found by Markevitch to produce a significant shift in cooling flow cluster temperatures relative to an isothermal fit to the combined spectrum. Other cluster temperatures, on the other hand, were unchanged.

Such temperatures are difficult to reproduce precisely in the simulations, mainly because the spatial extent and subdivision of *ASCA* images is different for each cluster in the sample (Markevitch et al. 1998) The large scale of *ASCA* spectral regions implies that the temperatures in each pixel are similar in character to the spectral temperatures described earlier, but with more weight given to the luminous core than the outer regions. I simulate these temperatures by dividing our observation windows into nine sectors with a morphology typical for *ASCA* clusters: a core region with radius $r_{500}/4$; an inner annulus surrounding this region with outer radius $5r_{500}/8$, and an outer annulus surrounding this region with outer radius r_{500}. The two annuli are each divided into 4 quadrants. The average spectral temperature T_s over all nine sectors, weighted by total energy flux, will be referred to as a *flux-weighted* temperature T_f for the remainder of this paper. This definition of T_f should not be confused with the emission-weighted temperature T_e described in ME01, which is the density-weighted average thermodynamic temperature calculated over a spherical volume. T_f is, however, closely comparable to the emission-weighted temperatures described in the Markevitch et al. (1998) analysis.

The deviation δT_f has a slope similar to that of δT_s (Equation 1), but a different normalisation:

$$\delta T_f \equiv \frac{T_v - T_f}{T_f} = (0.22 \pm 0.05) \log_{10} T_f [\mathrm{keV}] - (0.11 \pm 0.03). \quad (2)$$

T_f is generally higher than T_s because of the extra weight given to the core, but the scale-dependence of its deviation is similar. The mean value of δT_f ranges from about -10% for poor clusters to +10% for rich clusters with virial temperatures on the order of 10 keV. Calculating the flux-weighted mean temperature for a coarse grid does not free temperature measurements from a spectral bias due to the presence of multiple phases in a gas column, but it provides a more accurate estimate of the virial temperature for rich clusters.

The deviations between virial temperatures and observable spectral temperatures described in Equations 1 and 2 do not vary with cosmological model or evolutionary epoch, nor do they vary significantly when the radius of the observed region is increased to enclose an mean overdensity of 200 times the critical density. δT_s and δT_f are plotted agains T_s and T_f in Figure 1. These are robust measures of an observational bias arising from realistic density and temperature distributions in the ICM. SPH simulations have been shown to accurately reproduce the large-scale morphology of real clusters (Mohr et al. 1995), and a similar analysis of this particular ensemble displayed an even closer structural correspondence (Mohr & Evrard, private communication). N-body simulations of dark matter evolution have likewise been shown to produce merger histories which are in good agreement with Press-Schechter theory (Lacey & Cole 1994), so it is likely that these variations are similar in magnitude to those in real clusters. Analysis of Eulerian simulations reveals a similar level of clumping in the ICM (Bryan & Norman, private communication).

3   MODELING THE MASS FUNCTION

When converting a model mass function $n(M, z)$ to an observable XTF $n(T, z)$, it is generally assumed that the clusters formed at their observed redshift. Kitayama & Suto (1996) were the first relax this assumption in modeling the XTF, applying the techniques of Lacey & Cole (1993) to calculate realistic distributions of formation epochs for the clusters at a given redshift. They reasoned that clusters which formed significantly earlier than their observation epoch would be hotter than clusters of a similar mass which collapsed more recently. Cosmological scaling of the background mean density and temperature predicts a normalisation evolution in the mass-temperature relation proportional to $h(z)/h_0 = \sqrt{\Omega_{\mathrm{m}}(1 + z)^3 + \Omega_\Lambda}$ for a flat universe (e.g. Bryan & Norman 1998), and the temperature corrections for such clusters can therefore be rather large. Other groups have recently begun to take up this standard in modeling the temperature function and its evolution (Viana & Liddle 1999, Kay & Bower 1999), but this extension to the model is not yet justified by observations.

Making this correction implies an additional assumption, however: that the X–ray luminous regions of clusters
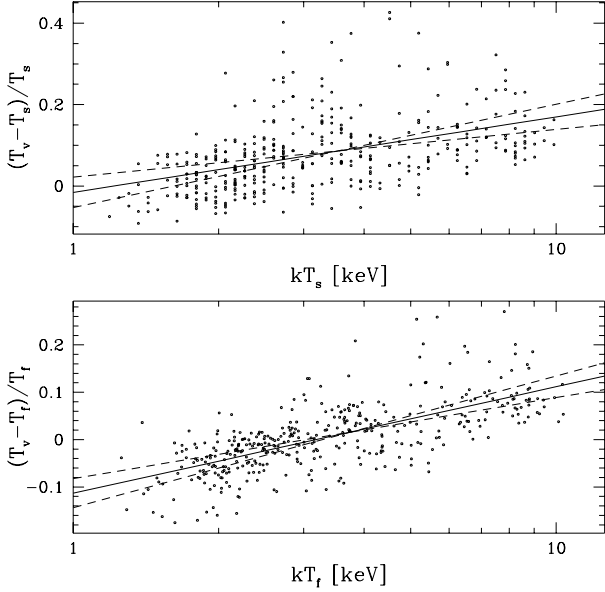
Figure 1. The upper panel displays the deviation δT_s between virial temperature and spectral temperature as a function of the spectral temperature. 384 points are displayed, corresponding to 16 evolutionary epochs of 24 independent cluster simulations. The best-fitting correlation between δT_s and T_s (Equation 1) is independent of redshift. The lower panel displays the corresponding relationship between δT_f and T_f, as reported in Equation 2. The dashed lines in each panel display one-sigma variations on the best-fitting correlations.

are approximately relaxed. Merger events have the potential to significantly alter a cluster's temperature when they occur, and they need not be very large to do so (Cavaliere et al. 1999, ME01). For a cluster which formed at high redshift to maintain a temperature appropriate for that epoch, it should have already accumulated most of its observed mass. The rate of mergers observed in simulations makes this scenario seem unlikely, although Kitayama and Suto cite results from Eulerian simulations (Bryan & Norman 1998) indicating that a cluster's temperature doesn't change much after its formation. We note that the temperature which they refer to is a simulation's luminosity-weighted temperature (similar to the T_e used in ME01), which is very similar to the core temperature of the gas. Observational measures of the temperature such as T_s and T_f are more heavily influenced by cool gas in the outer regions of the cluster, and more susceptible to minor merger events.

These simulations can be used to test the sensitivity of observable and virial temperatures to ongoing minor mergers. The mass of our clusters as a function of flux-weighted temperature is plotted in Figure 2, and presents a tight correlation with only 18% scatter:

$$\log_{10}(M_{tot}h(z)) = (1.66 \pm 0.04)\log_{10} T_f + (13.59 \pm 0.02). \quad (3)$$

This plot combines cluster outputs at redshifts $z = 1.0$, 0.5, and 0. The small degree of scatter in this plot strongly implies that there is no significant contamination of the tem-
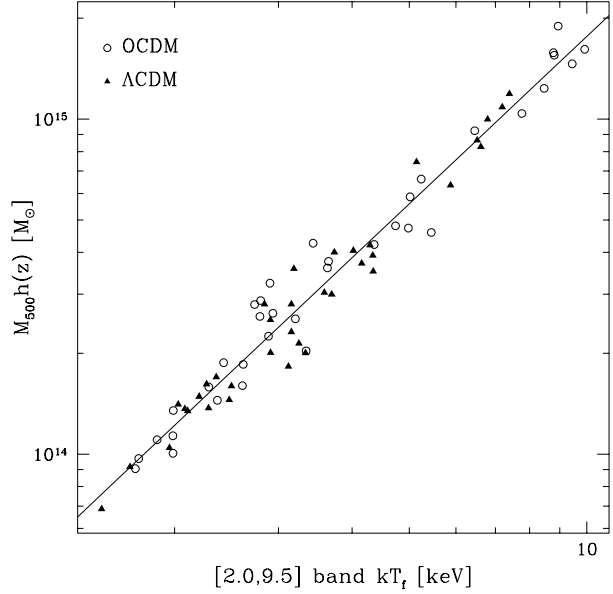

Figure 2. The relationship between flux-weighted temperature T_f and total mass measured within r_{500}. Clusters at redshifts 0.0, 0.5 and 1.0 are included in the plot, with masses scaled by the cosmological evolution factor h(z). The best-fitting relation is drawn, and its parameters are reported in Equation 3.

perature ensemble by clusters which virialized early; when scaled to a similar epoch the three relations $M(T_f; z)$ are identical. We can, however, probe this issue more deeply.

We define a cluster's formation epoch z_f as the redshift at which it has acquired $75\% \pm 7.5\%$ of its final mass, following the convention used by Viana & Liddle (1999) in their recent paper constraining cosmological parameters. If the extension of Kitayama & Suto is relevant to our interpretation of the local XTF, then we should see a correlation between cluster temperature and z_f: clusters with high formation redshifts should, on the average, have temperatures higher than the mean mass-temperature relation. Figure 3 plots this difference for virial, spectral, and flux-weighted temperatures within observation windows of radius r_{500} and r_{200}. Error bars along the z_f axis are given to objects which passed through the mass threshold with a significant component of continuous accretion, so that the cluster had between 67.5% and 82.5% of its final mass in more than one output frame. The uncertainties implied by these error bars are not used in the statistical analysis. All the best-fitting lines for the six data sets are consistent with zero slope, although it is fair to say that there is evidence for a slight positive correlation. On the other hand, this correlation is largely driven by the rare clusters which formed at very high redshifts; most of these objects formed at $z_f < 0.6$ and are evenly distributed about the mean mass-temperature relationship.

Correlation coefficients and best-fit line parameters for these data are summarized in Table 1. The correlations within r_{200} are significantly influenced by a cluster with a formation redshift of 0.8 and very large error bars on that
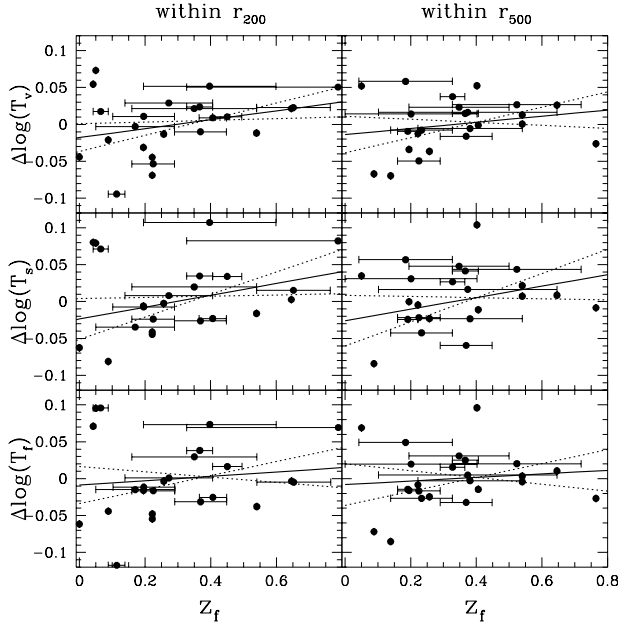
Figure 3. The best-fitting mass-temperature relationship $\bar{T}(M)$ is calculated for the 24 clusters in this ensemble at a redshift of zero, and the deviation of individual clusters from this relation $\Delta \log T \equiv log(T/\bar{T})$ is plotted against their formation redshift z_f. Three definitions of the temperature (virial, spectral, and flux-weighted) and two observation windows are examined. If the temperature of a cluster were strongly influenced by its formation epoch, we would expect to see a correlation between $\Delta \log T$ and z_f. The evidence for correlation in this data set is marginal at best, and negligible for the flux-weighted temperatures which are most similar to *ASCA* measurements. Although the simulated clusters display the expected cosmological evolution in the normalization of their mass-temperature relation, the scaling relation at zero redshift does not appear to be contaminated by clusters which virialized at earlier epochs.

Temperature		R	slope	intercept
r_{200}	T	0.31(15%)	0.060 ± 0.044	-0.018 ± 0.017
	T_s	0.28(20%)	0.080 ± 0.066	-0.024 ± 0.025
	T_f	0.12(58%)	0.030 ± 0.060	-0.009 ± 0.022
r_{500}	T	0.21(33%)	0.041 ± 0.051	-0.014 ± 0.020
	T_s	0.28(20%)	0.078 ± 0.086	-0.026 ± 0.034
	T_f	0.11(68%)	0.024 ± 0.057	-0.008 ± 0.022

Table 1. A correlation analysis of the data presented in Figure 3. R is the correlation coefficient of the data, and is also translated into the probability that an uncorrelated set of 24 random points would produce a correlation coefficient at least that large. The slope and intercept of the best-fitting lines plotting in Figure 3 are also given.

explicitly as evolving entities. One example of such a model has been presented by Cavaliere et al. (1999), who analyze ICM structure in terms of "punctuated equilibrium", a sequence of merger shocks followed by partial relaxation of the ICM to the shock boundary conditions. Their model agrees with these simulations in showing that minor merger events should have a more important influence on the evolution of ICM temperatures than major mergers, and makes some important predictions about the behavior of ICM scaling relations for rich groups and poor clusters.

4 CONCLUSIONS

An analysis of the evolutionary history of simulated clusters shows only a slight dependence of cluster temperature on formation epoch out to $z_f \sim 0.6$, although the small number of clusters in this ensemble leaves open the possibility of evolution in the temperatures of clusters which formed at high redshifts. It is also worth reiterating that when using a flux-weighted temperature T_f, which is the definition most appropriate to analysis of the cluster temperature function, this correlation essentially vanishes. This lack of dependence on formation epoch can be traced to a high frequency of smaller (mass ratio $\lesssim 25\%$) merger events, which introduce cool gas into the ICM and allow it to approach an equilibrium appropriate to the merger epoch. This work implies that extending analysis of the temperature function to account for the difference between a cluster's formation and observation redshifts is not necessary in a dynamically young halo population.

value. This cluster acquired most of its mass very early in the simulation and grew through gradual accretion thereafter, so the reshift range during which it had a mass of 75%±7.5% its final mass is very long. It's temperature, while higher than the ensemble average, is well within the variations seen for more recently formed clusters. If this point is left out the analysis, then all the slopes become consistent with zero in their one-sigma uncertainty range, and the correlation coefficients drop to 0.24 (T_v), 0.19 (T_s), and 0.005 (T_f). These coefficients correspond respectively to 32%, 39%, and 100% probabilities of uncorrelated data.

The discrepancy between our intuition (clusters which first virialized at an early epoch should be hotter) and these simulations can be resolved by acknowledging the essentially dynamic nature of clusters in a low-density universe. Multiple lines of observational evidence point to an $\Omega_m \sim 0.3$ cosmology in which clusters are still forming at the present day, and the theoretical construct of a relaxed, virialized cluster seems to have few counterparts in the observable population. Rather than treating clusters as static fossils of the primordial density field, we should attempt to model them

REFERENCES

Bialek J. J., Evrard A. E., & Mohr J. J., 2001, preprint (astro-ph/0010584)
Bond J. R. & Efstathiou G., 1984, ApJL, 285, L45

Bond J. R., Cole S., Efstathiou G., & Kaiser N., 1991, ApJ, 379, 440

Bryan G. L. & Norman M. L., 1998, ApJ, 495, 80

Cavaliere A., Menci N., & Tozzi P., 1998, ApJ, 501, 493

Cavaliere A., Menci N., & Tozzi P., 1999, MNRAS, 308, 599

Chièze J.-P., Alimi J.-M. & Teyssier R., 1998, ApJ, 495, 630

Henry, J. P., 2000, ApJ, 534, 565

Jenkins A., Frenk C. S., White S. D. M., Colberg J. M., Cole S., Evrard A. E., & Yoshida N., 2000, preprint (astro-ph/0005260)

Kay S. T. & Bower R. G., 1999, MNRAS, 308, 664

Kitayama T. & Suto Y., 1996, ApJ, 469, 480

Kitayama T. & Suto Y., 1997, ApJ, 490, 557

Lacey C. & Cole S., 1993, MNRAS, 262, 627

Lacey C. & Cole S., 1994, MNRAS, 271, 676

Lloyd-Davies E. J., Ponman T. J. & Cannon D. B., 2000, MN-RAS, 315, 689

Markevitch M., 1998, ApJ, 504, 27

Markevtich M., Forman W. R., Sarazin C. L., & Vikhlinin A., 1998, ApJ, 503, 77

Mathiesen B. F. & Evrard A. E., 2001, ApJ, in press (astro-ph/0004309)

Metzler C. A. & Evrard A. E., 1994, ApJ, 437, 564

Mewe R., Lemen J. R., & van den Oord G. H. J., 1986, A&AS, 65, 511

Mohr J. J., Evrard A. E., Fabricant D. G., & Geller M. J., 1995, ApJ, 447, 8

Mohr J. J. & Evrard A. E., 1997, ApJ, 491, 38

Mohr J. J., Mathiesen B. F., & Evrard A. E., 1999, ApJ, 517, 627

Press W. H. & Schechter P., 1974, ApJ, 187, 425

Sheth R. K., Mo H. J., & Tormen G., 1999, preprint (astro-ph/9907024)

Takizawa, M. 1999, ApJ, 520, 514

Viana P. T. P. & Liddle A. R., 1999, MNRAS, 303, 535